energies

MDPI

Article

A DCM-Based Non-Isolated Step-Down DC Transformer

Minseung Kim [1], Donghee Choi [2] and Soo Hyoung Lee [3,*]

[1] Department of Electrical Engineering, Mokpo National University, Muan 58554, Republic of Korea
[2] Division of Converged Electronic Engineering, Cheongju University, Cheongju 28503, Republic of Korea; heechoi@cju.ac.kr
[3] Division of Electrical, Electronic, and Control Engineering, Kongju National University, Cheonan 31080, Republic of Korea
* Correspondence: lsh@kongju.ac.kr

Abstract: DC transformers have emerged as essential devices for medium voltage DC (MVDC)-low voltage DC (LVDC) distribution systems. However, conventional step-down single-level converters have limits on the voltage level of the MVDC-LVDC distribution system. This paper proposes a non-isolated step-down (NISD) DC transformer based on discontinuous conduction mode (DCM). The proposed structure can withstand high voltage levels by sharing voltages between energy storage modules dividing voltage levels. The proposed NISD DC transformer determines operational modes based on energy storage modules and performs the voltage conversion process. The effectiveness of the proposed NISD DC transformer is verified based on a case study using a power system computer-aided design and electromagnetic transient simulation engine including DC (PSCAD/EMTDC™).

Keywords: DC distribution; DC transformer; modular multilevel converter; non-isolated converter; step-down converter

Citation: Kim, M.; Choi, D.; Lee, S.H. A DCM-Based Non-Isolated Step-Down DC Transformer. *Energies* **2024**, *17*, 940. https://doi.org/10.3390/en17040940

Academic Editors: Wenzhong Ma, Xingtian Feng and Shuguang Song

Received: 4 January 2024
Revised: 5 February 2024
Accepted: 15 February 2024
Published: 17 February 2024

1. Introduction

As climate change poses increasingly significant environmental challenges, there is a worldwide increase in the demand for renewable sources of energy that are sustainable and environmentally friendly. In accordance with the International Energy Agency, renewable energy will comprise 29.8% of the world's overall electricity production by 2022 [1]. The growth of direct current (DC) power generation is driving the increase in renewable energy production, along with the rise of DC loads such as electric vehicle charging stations and data centers [2–4]. This attention is leading to a focus on DC power transmission and distribution [2–7]. A critical challenge in this area is the design of converters to reduce the voltage level from medium-voltage DC (MVDC) to low-voltage DC (LVDC) without using the bulky and expensive AC transformers that are currently in use. A DC transformer, commonly known as a DC-DC converter, uses switching components and energy storage implements for voltage transformation [8,9]. However, conventional single-stage step-down converters require high-rated voltages for each component, which leads to higher costs, larger sizes, and higher losses. As a consequence, the MVDC to LVDC distribution voltage levels are limited [10–12].

To overcome the disadvantages of replacing AC transformers, alternative isolated DC converters using medium- or high-frequency transformers have been proposed instead of the traditional bulky low-frequency transformers [13–16]. Despite this solution, these converters still exhibit certain drawbacks, such as losses during the DC-AC-DC conversion and the continued presence of AC transformers [17].

This paper proposes a non-isolated step-down (NISD) DC transformer based on discontinuous conduction mode (DCM). Currently, only DCM operation is considered, and the proposed structure divides high voltage using an energy storage module (ESM) comprised of series. The proposed NISD DC transformer determines operational mode based on the ESMs and performs voltage transformation, providing the following advantages:

(1) It is possible to achieve a high voltage ratio with a small number of components and a simple control method.
(2) It operates in DCM, reducing switching losses and improving efficiency.
(3) There is no requirement for an isolation transformer or galvanic isolation, which results in reduced cost and size.

The proposed NISD DC transformer uses capacitors to store electric energy in ESMs [18–27], unlike the conventional DC converter that uses inductors to store magnetic energy and perform voltage conversion [3,6,15,16,18,19,28–32]. Also, conventional flying capacitor multilevel converters have complex control schemes [24–26] in contrast to this structure, enabling flexible control of the output voltage by adjusting the charge and discharge duty of ESMs. The high voltage of MVDC is dispersed among ESMs, allowing for a reduction of each circuit element's rated voltage to the level of commonly used components. Currently, soft switching is considered for the only main switches excluding ESMs.

The remaining parts of this paper are structured as follows: Section 2 presents the topology and configuration of the proposed NISD DC transformer, as well as its operational modes and control strategy. Section 3 analyzes the IGBT voltage stress and current as well as the considerations for the inductor, ESM, and output capacitor during the design of the proposed NISD DC transformer. Section 4 provides the results of simulations conducted using a power system computer-aided design and electromagnetic transient including DC (PSCAD/EMTDC) to validate the effectiveness of the proposed NISD DC transformer in two cases: the steady state and with disturbances. Finally, Section 5 summarizes the key contributions of this paper and proposes several future research directions.

2. NISD DC Transformer Based on DCM

2.1. NISD DC Transformer Topology

The topology of the non-isolated step-down DC transformer is presented in Figure 1. The proposed topology operates based on capacitors in contrast to the conventional one that uses an inductor. It includes n energy storage modules for voltage transformation and operates according to a six-duty ratio segment mode. Each energy storage module is composed of a capacitor, marked as (C), and two insulated gate bipolar transistors (IGBTs), labeled as (S_a, S_b), which are charged and discharged by separate groups of IGBTs, marked as (S_{11}, $\cdots$, $S_{1\alpha}$ and S_{21}, $\cdots$, $S_{2\alpha}$). Moreover, the addition of the inductor (L) and the output capacitor (C_{out}) restrict excessive current and reduce the ripple in output voltage, respectively.

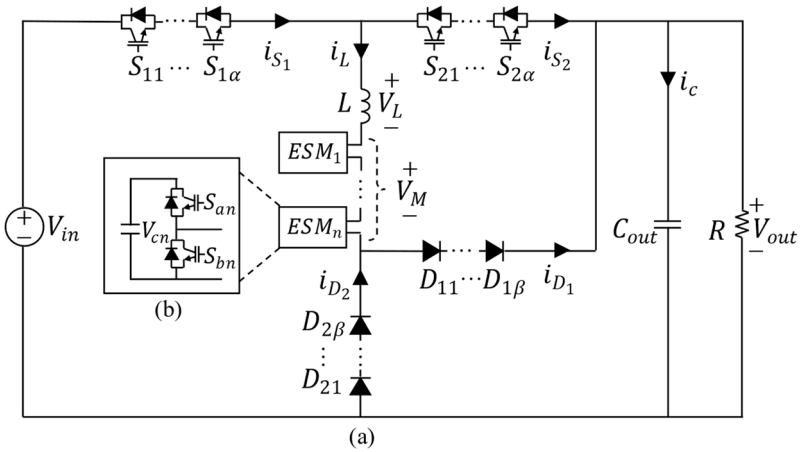

Figure 1. (**a**) NISD DC transformer topology including (**b**) ESM.

2.2. Operational Modes

The operational modes of the NISD DC transformer are composed of duty cycles divided into six segments ($M_1 - M_6$) based on the charging and discharging of the inductor and ESM. The operational sequence depicted in Figure 2 is demonstrated to operate in a

steady state. The waveforms of voltage and current are periodic, with identical values at the beginning (t_0) and end (t_6) of each cycle. Figure 3 illustrates the NISD DC transformer's operational mode for each segment. And its current path is shown as red highlighted.

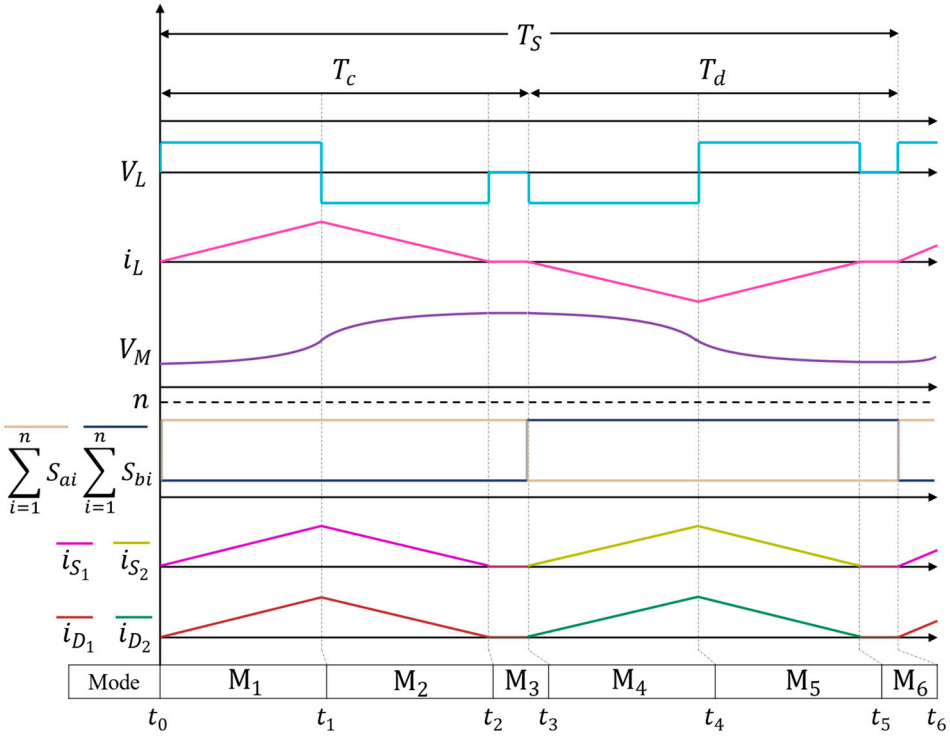

Figure 2. Operational sequences of the proposed DC transformer.

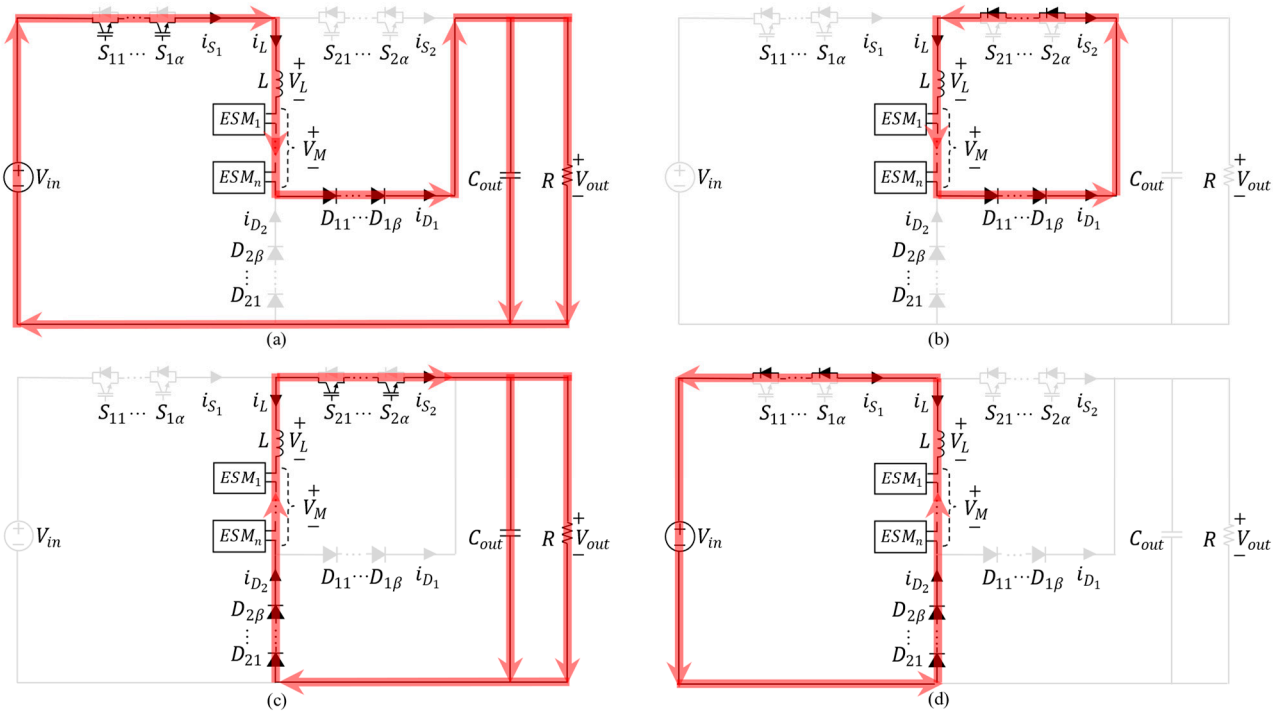

Figure 3. Operational modes of NISD DC transformer: (**a**) M_1, (**b**) M_2, (**c**) M_4, (**d**) M_5.

Before analyzing each operational mode, it is assumed that the IGBTs, diodes, and ESMs' capacitor balancing are ideal during operation. Moreover, the inductor has low

inductance to make the inductor current periodically zero, and each capacitor is assumed to have a large enough capacitance to maintain a constant voltage at the output voltage V_{out} and the voltage V_{cn} $(n \in \mathbb{N})$ of each ESM.

The voltage reference of the ESM capacitor is defined by the relationship between the input voltage and the number of ESMs, as shown in (1).

$$V_c = \frac{V_{in}}{n} \tag{1}$$

The average of each ESM capacitor voltage is expressed as (2), and the operational mode is determined by the relationship between (1) and (2).

$$\overline{V_c} = \frac{1}{n}\sum_{i=1}^{n} V_{ci} \tag{2}$$

2.2.1. First Operational Mode $M_1 : (t_0 - t_1)$

During the steady state, the state at t_0 is identical to the state at t_6 in the prior operational sequence., i.e., both groups of IGBTs are off and the inductor current is zero. Afterward, IGBT group 1 ($S_{11}, \cdots, S_{1\alpha}$) is turned on, which causes the capacitor of the ESM to charge and the voltage to increase through the path, as shown in Figure 3a. During this process, the inductor prevents an overcurrent by filling the difference between the input voltage and the controlled ESM voltage and V_M, as shown in (3).

$$V_L = V_{in} - V_M - V_{out} \tag{3}$$

2.2.2. Second Operational Mode $M_2 : (t_1 - t_2)$

During the first operational mode, when the voltage charged to each ESM is sufficiently high to satisfy $\overline{V_c} > V_c$, the IGBT group 1 ($S_{11}, \cdots, S_{1\alpha}$) is turned off at t_1. At this moment, as illustrated in Figure 3b, current that has been charged to the inductor by circulating through the antiparallel diodes of IGBT group 2 ($S_{21}, \cdots, S_{2\alpha}$), the ESM, and diode group 1 ($D_{11}, \cdots, D_{1\beta}$) delivers energy to ESMs and then discharges to zero. At this time, the voltage of each ESM capacitor is increased by the ESM capacitor's voltage ripple ΔV_c to the reference voltage in (1) to $V_c + \Delta V_c$. The inductor voltage during discharge in this mode is determined by (4).

$$V_L = -V_M \tag{4}$$

2.2.3. Third Operational Mode $M_3 : (t_2 - t_3)$

As the load on the DC transformer approaches its maximum rated load, which is $M_3 = 0$ at full load, the duration of the third mode is reduced. However, its changes do not affect the stability of the output voltage considering the fixed switching frequency.

2.2.4. Fourth Operational Mode $M_4 : (t_3 - t_4)$

In the third operational mode, after the inductor current is completely discharged and IGBT group 2 ($S_{21}, \cdots, S_{2\alpha}$) turns on at t_3, the ESM capacitor discharges via the path shown in Figure 3c and the voltage decreases. As in the first mode, the inductor prevents overcurrent by covering the gap between the controlled ESM voltage and the output voltage, as given by (5).

$$V_L = V_{out} - V_M \tag{5}$$

2.2.5. Fifth Operational Mode $M_5 : (t_4 - t_5)$

After the ESM is discharged in the fourth mode and the voltage is sufficient to satisfy $\overline{V_c} < V_c$, IGBT group 2 ($S_{21}, \cdots, S_{2\alpha}$) is turned off at t_4. At this point, the inductor current that has been accumulated is diverted back to the input side and discharged to zero through the anti-parallel diodes of IGBT group 2 ($S_{21}, \cdots, S_{2\alpha}$), the ESM, and diode group 2 ($D_{21}, \cdots, D_{2\beta}$), as seen in Figure 3d. At this time, the ESM capacitors are continuously

being discharged to reduce the voltage to $V_c - \Delta V_c$ according to the previous mode, and the voltage of the discharged inductor is equal to (6).

$$V_L = V_{in} - V_M \tag{6}$$

2.2.6. Sixth Operational Mode $M_6 : (t_5 - t_6)$

Similar to the third operational mode, when the DC transformer operates at full rated load, then $M_6 = 0$. The duration of the sixth operational mode is also longer when operating at lower load.

2.3. Control Strategy

The control logic of the NISD DC transformer is presented in Figure 4. Thereafter, it proceeds in sequence through the six operational modes detailed in Section 2.2. At the outset, the voltage of the ESM begins at zero; therefore, IGBT group 1 (S_{11}, $\cdots$, $S_{1\alpha}$) is turned on and operates as M_1. Subsequently, IGBT group 1 (S_{11}, $\cdots$, $S_{1\alpha}$) and IGBT group 2 (S_{21}, $\cdots$, $S_{2\alpha}$) are controlled by the voltage of ESMs, and the charging and discharging of ESMs are determined according to the six operational modes described in Section 2.2.

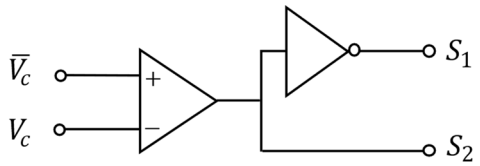

Figure 4. Control logic for IGBT group.

The total inserted voltage of the ESMs, V_M, in Figure 3, is determined by the number of ESMs inserted in each operational mode, N, and the capacitor voltage of the inserted ESM, according to (7). Additionally, capacitor balancing causes the ESM charging duty, V_{ci} at T_c, to be sorted in ascending order while the ESM discharging duty, V_{ci} at T_d, is sorted in descending order to ensure that the capacitor voltage of all ESMs is constantly charged and discharged.

$$V_M = \sum_{i=1}^{N} V_{ci} \tag{7}$$

At this time, the number of ESMs to be inserted N depends on N_{ctrl}, which is controlled by the output voltage, and a number of total modules n, which is determined by the specification of the NISD DC transformer. Therefore, the number of inserted ESMs N according to the charging and discharging cycle of the ESM is determined as (8). Also, as the ratio of input voltage to output voltage increases, the change of N, i.e., V_M, increases.

$$N = \begin{cases} n - N_{ctrl} & for\ T_c \\ N_{ctrl} & for\ T_d \end{cases} \tag{8}$$

Depending on the operational mode, the ESM is inserted to charge and discharge, and the output voltage is determined by M_1 and M_4. In order to effectively regulate the output voltage, the ESM must be inserted variably, and the control variable N_{ctrl} of the insertion number is controlled flexibly according to the output voltage. N_{ctrl} is calculated via the control diagram shown in Figure 5, and an additional insertion amount is calculated through the PI controller for error correction of the output voltage. The insertion amount is limited to a minimum of 1 and a maximum of $n - 1$ for the operation described in Figure 3. Since the number of modules is an integer, the amount of insertion is selected by converting to UInt (Unsigned Integer) type.

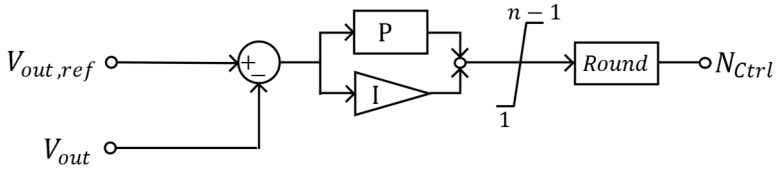

Figure 5. Control diagram for ESM insertion amount.

2.3.1. ESM Charging Duty (T_c)

Using (3) and (4), the voltage output during the ESM charging period at T_c is calculated from (9). At this time, the total inserted voltage of the ESMs, V_M between M_1 and M_3 is determined by (7) and (8).

$$V_{out} = V_{in} - \frac{t_2 - t_0}{t_1 - t_0} V_M \tag{9}$$

Meanwhile, the relationship between the output voltage V_{out} and the number N_{ctrl} of ESMs inserted while the ESMs are charging is shown in Figure 5. If the output voltage is higher than the reference voltage, additional modules are inserted to charge the ESMs and, simultaneously, the high electrical voltage difference between the input and output is reduced, i.e., if the output voltage is higher than the reference voltage, N_{ctrl} is reduced to increase the inserted number of ESMs, N. Alternatively, if the output voltage is lower than the reference voltage, N is reduced to control the output voltage.

2.3.2. ESM Discharging Duty (T_d)

The voltage output during the T_d discharge period of the ESM is obtained by utilizing (5) and (6), as demonstrated in (10). Similarly to T_c, (7) and (8) are applied to determine V_M in the M_4 to M_6 range.

$$V_{out} = \frac{t_5 - t_3}{t_4 - t_3} V_M - \frac{t_5 - t_4}{t_4 - t_3} V_{in} \tag{10}$$

The correlation between the output voltage V_{out} during the discharge of the ESMs and the control variable N_{ctrl} of the number of ESMs inserted is shown in Figure 5. The number of inserted ESMs, N, decreases when the output voltage is higher than the reference voltage, and, contrary to T_c, the number of inserted ESMs, N, decreases. As a result, the voltage source of the ESMs is reduced and the output voltage decreases. Conversely, as the output voltage is lower than the reference voltage, N_{ctrl} increases, which increases the number of ESMs inserted, and the output voltage is increased by the discharging ESMs.

3. Design Consideration of NISD DC Transformer

In this section, design considerations are provided for the implementation of the NISD DC transformer based on DCM. The energy conversion process is performed by multiple ESMs, including capacitors in the NISD DC transformer, and the overcurrent that can be produced by voltage unbalance during the conversion process is limited by inductors. Moreover, the capacitor on the output side reduces the ripple in output voltage.

Before analysis, Figure 2 demonstrates that when the NISD DC transformer operates by segments for $t_2 - t_0 > T_c$, i_L interrupts the ESM's capacitor discharge and load current in the T_d duty, which is not discharged in the T_c duty (i.e., $i_L > 0$). Similarly, when $t_5 - t_3 > T_d$, i_L interrupts the ESM's capacitor charge and load current in the T_c duty, which is not discharged in the T_d duty (i.e., $i_L < 0$). In both cases, the regular operation of the NISD DC transformer is interrupted, i.e., the theoretical maximum power transfer condition is $t_2 = t_3$ & $t_5 = t_6$, and when a load with more than the maximum power is connected, the output is reduced to protect itself from overcurrent. To ensure efficient operation, it is necessary for the maximum value I_{max} and minimum value I_{min} of the inductor current i_L to satisfy the condition $I_{max} = -I_{min}$, regarding the power loss I^2R in the conductor.

The values are determined by the switching frequency f_S of Group 1 ($S_{11}, \cdots, S_{1\alpha}$) and Group 2 ($S_{21}, \cdots, S_{2\alpha}$) IGBTs in Figure 1a and the switching frequency f_M of the two

IGBTs (S_a, S_b) of the ESM in Figure 1b, which are influenced by the inductor current i_L at rated load conditions. Thus, in this section, the relationship among f_S, f_M, the inductor and capacitors and the quantity of input and output voltages, IGBTs and diodes, and ESMs in a NISD DC transformer will be discussed.

3.1. Voltage Stress on IGBTs and Diodes

IGBTs and diodes are arranged in groups of α and β (α, $\beta \in \mathbb{N}$), respectively, to endure high voltages. IGBTs and diodes are controlled to operate, as shown in Figure 3, for voltage transformation.

IGBT Group 1 (S_{11}, $\cdots$, $S_{1\alpha}$) and Group 2 (S_{21}, $\cdots$, $S_{2\alpha}$), comprising α IGBTs, alternate in turning on/off to prevent short-circuiting of the NISD DC transformer. The voltage applied to the component when each IGBT group is operating is expressed as (11) and (12).

$$V_{S1} = V_{in} + V_{D2} - V_L - V_M \tag{11}$$

$$V_{S2} = V_{in} - V_{S1} - V_L \tag{12}$$

Diode groups 1 (D_{11}, $\cdots$, $D_{1\beta}$) and 2 (D_{21}, $\cdots$, $D_{2\beta}$) are composed of β diodes and perform opposite operations depending on the charging and discharging duty of the ESM. The voltage for each diode group is shown as (13), and, according to the equation, the reverse voltage during the reverse bias of the diode is mainly affected by V_{out}, and the voltage during the forward bias is operated to zero by the reverse voltage of the other diode group.

$$V_{D1} + V_{D2} = -V_{out} \tag{13}$$

In the design of the NISD DC transformer, the number of IGBTs and diodes is determined by $V_{in,ref}$ and $V_{out,ref}$, which are the reference of input and output voltages. From Figure 3, each group of components is organized and operated in series, so the number of IGBTs and diodes (α, β) for the rated voltage is determined as shown in (14) and (15).

When the rated collector-to-emitter voltage of an IGBT device is V_S, then

$$\alpha \geq \frac{V_{in,\,ref}}{V_S} \tag{14}$$

When the rated breakdown voltage of a diode device is V_D, then

$$\beta \geq \frac{V_{out,\,ref}}{|V_D|} \tag{15}$$

3.2. Current Calculations of IGBTs and Diodes

During operation, the IGBTs and diodes in each group are organized in series, as shown in Figure 3; thus, the current in each component within the same group is the same and is expressed as (16) and (17).

$$I_{S1} = I_{D1} = \begin{cases} I_L & for\ T_c \\ 0 & for\ T_d \end{cases} \tag{16}$$

$$I_{S2} = I_{D2} = \begin{cases} 0 & for\ T_c \\ -I_L & for\ T_d \end{cases} \tag{17}$$

3.3. Design on Inductor

The NISD DC transformer's inductor is installed to reduce the overcurrent that may occur when switching IGBTs' operation in accordance with the operating modes in relation to each duty ratio, and the inductance for the NISD DC transformer to operate can be calculated

by the total voltage of the inserted ESM (7), which is calculated from the inductor voltage in (6) and the number of ESM inputs in this mode (8), and is calculated as shown in (18).

$$L = \frac{(n - N_{ctrl})N_{ctrl}V_{in}(nV_{out} - N_{ctrl}V_{in})}{n^3 I_{min} f_S (V_{out} - V_{in})} \tag{18}$$

3.4. Design on Capacitor

The capacitors in the NISD DC transformer can be categorized into two types: the internal capacitors of the ESM responsible for transforming energy and the capacitors aimed at reducing the output voltage's ripple.

The ESM's internal IGBTs (S_a, S_b), which are composed of n in series, regulate the ripples in ESM's voltage ΔV_M by operating at a switching frequency f_M. The capacitance C_M of the ESM's internal capacitor can be calculated using (19).

$$C_M = \frac{I_{max}(n - N_{ctrl})}{2n\Delta V_M f_M} \tag{19}$$

IGBT groups 1 (S_{11}, $\cdots$, $S_{1\alpha}$) and 2 (S_{21}, $\cdots$, $S_{2\alpha}$) operate at a switching frequency f_S, and their respective operational modes are determined. From this, the output capacitor current I_c and output voltage's ripple ΔV_{out} are determined, and the capacitance of the output capacitor C_{out} configured in parallel with the output terminal is expressed with (20).

$$C_{out} = \frac{I_c N_{ctrl}}{2n\Delta V_{out} f_S} \tag{20}$$

4. Case Studies

In this section, to verify the proposed NISD DC transformer, a DC transformer with an input voltage of 35 kV, an output voltage of 1.5 kV, and a rated power of 1 MW is configured with 35 ESMs. Moreover, the switching frequency is set to 5 kHz, and the ESM switching frequency is set to 50 kHz. In addition, the overcurrent limit inductor is 40 μH, the capacitance of each ESM is 20 mF, the output capacitor is 1.45 mF, and the simulation parameters are configured as shown in Table 1. The simulation is performed as shown in Figure 1 using PSCAD/EMTDC. Additionally, the performance of the control method for the capacitor's voltage is confirmed through seven cases.

Table 1. Parameters of the NISD DC transformer.

Symbol	Quantity	Value
V_{in}	Input voltage	35 kV
V_{out}	Output voltage	1.5 kV
P	Rated power	1 MW
n	Number of ESMs	35
f_S	Switching frequency	5 kHz
f_M	ESM switching frequency	50 kHz
L	Inductance	40 μH
C_{out}	ESM capacitance	20 mF
C_M	Output capacitance	1.45 mF

Figure 6a demonstrates that the output voltage is verified at 1.5 kV—with the output power being 1 MW and the output current at 0.667 kA—to achieve the rated power of 1 MW. Furthermore, ESM's insertion control variable N is regulated based on operational modes, with a range of 1 to 34, and the total injected voltage V_M of the ESM according to N is properly operated according to (7). The relationship between the current in the IGBTs and diodes and the inductor's current is also validated to perform the same as shown in Figure 2—(16) and (17). The voltage applied to the IGBTs and diodes is also validated using a simulation, and the voltages in (11)–(13) are verified.

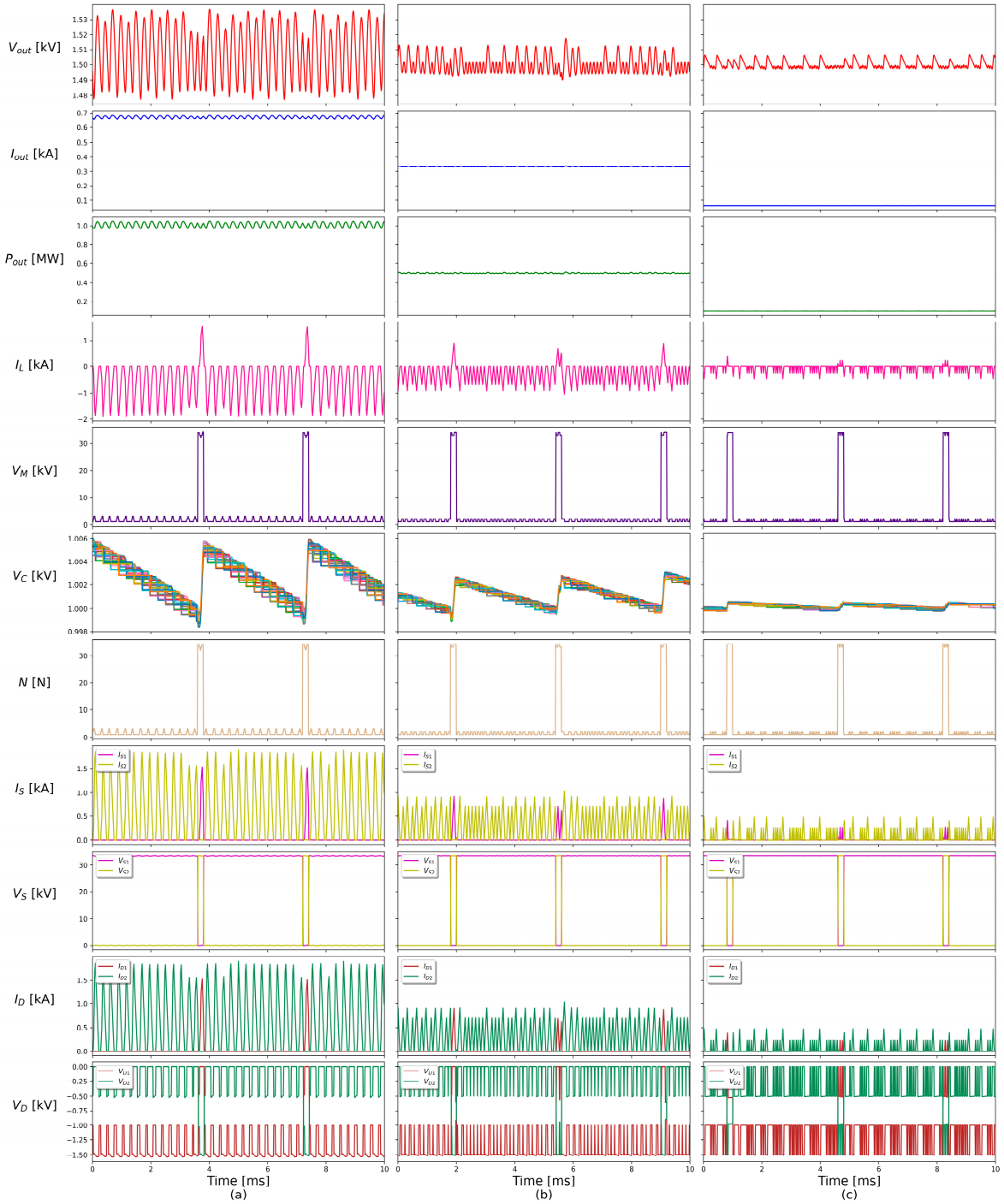

Figure 6. NISD DC transformer operation at resistive load of (**a**) 100%, (**b**) 50%, and (**c**) 10%.

4.1. Operations in Steady State

The NISD DC transformer is verified using constant resistive loads of 100%, 50%, and 10% (Figure 6a–c). The output voltage's ripples decrease by 3.904%, 1.44%, and 0.651%, respectively, as the load rate is reduced. Correspondingly, the output power's ripples decrease by 7.841%, 4.326%, and 1.304%, while the output voltage remains at 1.5 kV. The operational modes demonstrated consistency with the theoretical expectations, as the operating times of operational modes M_3 and M_6 increased with a decrease in load.

4.2. Operations with Disturbances

The simulation results, depicted in Figure 7a, illustrate normal output voltage control under the weak input voltage condition while operating under a 100% resistive load. in addition, the analysis of the figure indicates that the inductor current I_L is also influenced by the input at M_2, when compared to Figure 6a, at a weak input voltage.

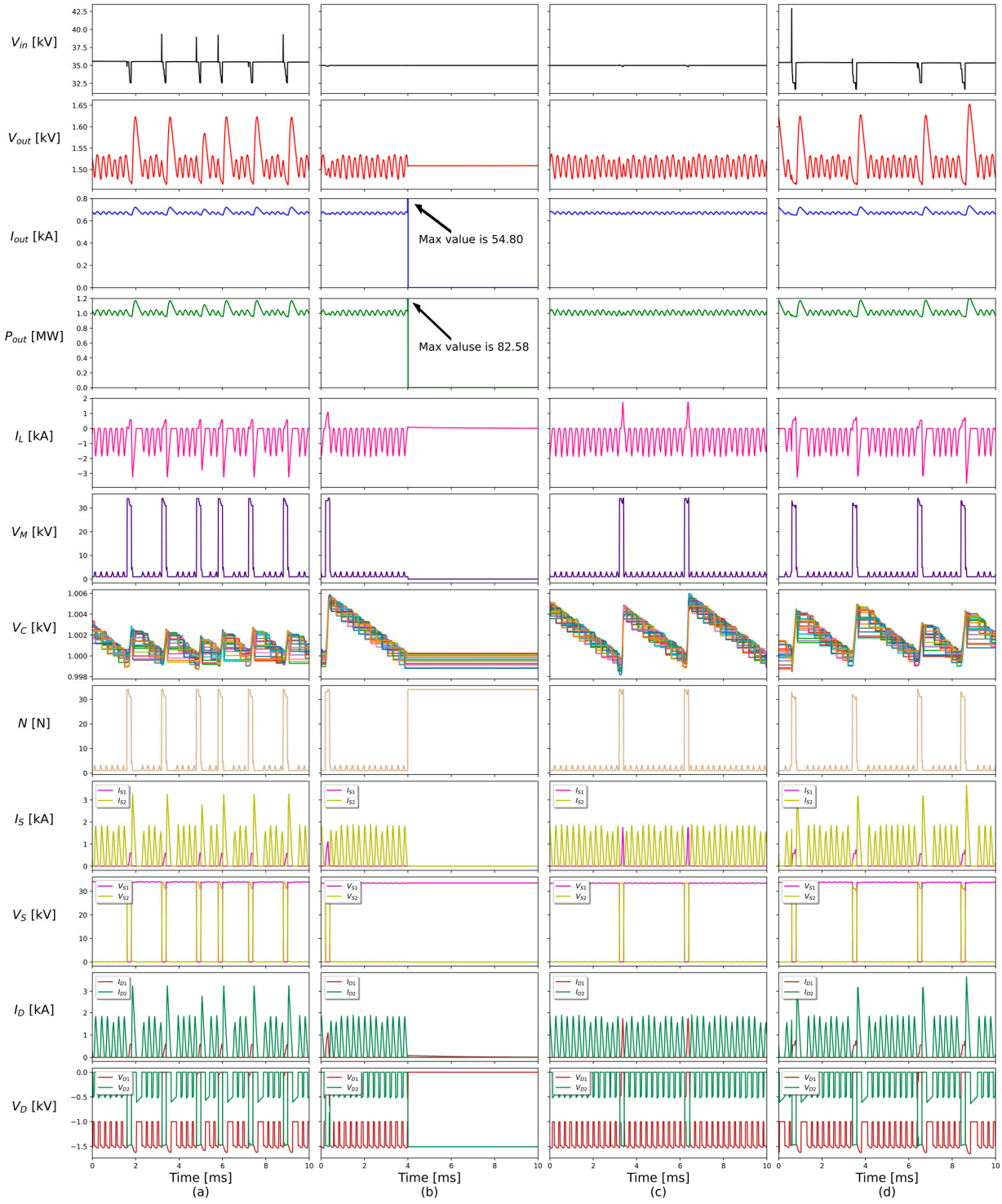

Figure 7. NISD DC transformer operation with (**a**) ripples in input voltage, (**b**) low-voltage side fault at 4 ms, (**c**) transition at 4 ms from 100% resistive to inductive load, and (**d**) transition at 4 ms from 100% resistive to inductive load during ripples in input voltage.

Next, in order to verify the operation and blocking ability in case of the LVDC side fault, a LVDC side fault was generated at 4 ms during an operation under 100% load, and the circuit breaker was opened 2 ms later to clear the fault (Figure 7b). Although, in this case, the fault current and power from the capacitor, C_{out}, increase to 54.80 kA and 82.58 MW, respectively. Such increases are a common problem for all inverters without a special protection scheme for an output capacitor. This might be solved by adding additional circuits, such as a damping resistor. Meanwhile, the rapid fault current reduction of the proposed converter based on the reduced capacitor size equates to a shorter discharge time with the same current compared to the other converters. At this time, all IGBTs were not damaged by immediately being opened. They cause the current and power to drop to zero and trigger sequential operations of the circuit breaker. Therefore, the proposed NISD DC transformer should be shortened. Inside the NISD DC transformer, the operation is similar to the second operational mode M_2, since all IGBTs are opened, and the voltage, V_{D2}, of diode group 2 is applied through the anti-parallel diode of IGBT group 2 and the diode of the ESM.

To evaluate the performance of the transformer during the rapid load changes of the power system, an inductance of 0.1 H was transitioned at 4 ms while operating at 100% resistive load rate (Figure 7c). This representatively reflects the aggregated effect caused by independent changes of various loads located through different feeders, and the system is stable.

Finally, the inductance was transitioned at 4 ms with high-impedance input voltage, i.e., the conditions in Figure 7a,c were considered simultaneously. Therefore, a weak input voltage causes the output current to ripple up to 8.077% due to the discharge of the capacitor, and the output power to ripple up to 15.728%. Although the inductor current is affected, it operates between 0.798 kA and −2.819 kA. Thus, it does not cause a problem for IGBT group 1 (S_{11}, $\cdots$, $S_{1\alpha}$) and 2 (S_{21}, $\cdots$, $S_{2\alpha}$) and diode group 1 (D_{11}, $\cdots$, $D_{1\beta}$) and 2 (D_{21}, $\cdots$, $D_{2\beta}$). Also, the increase in the ripple of output voltage is negligible. As shown in Figure 7d, the NISD DC transformer operates reliably, even in harsh conditions.

5. Conclusions

This article proposed a non-isolated step-down (NISD) DC transformer based on DCM for the MVDC-LVDC distribution system. To verify the performance of the proposed NISD DC transformer, normal operation was confirmed with loads of 100%, 50%, and 10%. Additionally, abnormal situations such as inductive load, LVDC side fault, and instability input voltage were assumed and simulated using a power system computer-aided design and electromagnetic transient simulation engine including DC (PSCAD/EMTDC). The proposed NISD DC transformer successfully operated for the purpose of energy transformation.

This study verified the performance of energy transformation from MVDC to LVDC, i.e., the MVDC-LVDC distribution system. However, further studies are required to apply the proposed NISD DC transformer to an HVDC-MVDC system or step-up version of the proposed transformer, even a bidirectional one.

Author Contributions: Conceptualization, S.H.L.; methodology, S.H.L. and D.C.; software, M.K.; validation, S.H.L. and M.K.; formal analysis, S.H.L. and M.K.; investigation, S.H.L. and M.K.; resources, S.H.L. and M.K.; data curation, S.H.L. and M.K.; writing—original draft preparation, M.K.; writing—review and editing, S.H.L.; visualization, M.K.; supervision, S.H.L. and D.C.; project administration, S.H.L.; funding acquisition, S.H.L. and D.C. All authors have read and agreed to the published version of the manuscript.

Funding: This work was supported in part by the National Research Foundation of Korea (NRF) funded by the Korean Government (MSIT) under grant 2022R1A2C2006688, and in part by the Basic Science Research Program through the National Research Foundation of Korea (NRF) funded by the Ministry of Education (2022R1C1C1005975).

Data Availability Statement: The datasets presented in this article are not readily available because the data are part of an ongoing study.

Conflicts of Interest: All of the authors declare that they have no known competing financial interests or personal relationships that could have appeared to influence the work reported in this paper.

References

1. Enerdata. *Global Energy Trends 2023*; Enerdata: Grenoble, France, 2023.
2. Suryadevara, R.; Parsa, L. Full-Bridge ZCS-Converter-Based High-Gain Modular DC-DC Converter for PV Integration with Medium-Voltage DC Grids. *IEEE Trans. Energy Convers.* **2019**, *34*, 302–312. [CrossRef]
3. Lu, Z.; Li, C.; Zhu, A.; Luo, H.; Li, C.; Li, W.; He, X. Medium Voltage Soft-Switching DC/DC Converter with Series-Connected SiC MOSFETs. *IEEE Trans. Power Electron.* **2021**, *36*, 1451–1462. [CrossRef]
4. Jin, H.; Chen, W.; Hou, K.; Shao, S.; Shu, L.; Li, R. A Sharing-Branch Modular Multilevel DC Transformer with Wide Voltage Range Regulation for DC Distribution Grids. *IEEE Trans. Power Electron.* **2022**, *37*, 5714–5730. [CrossRef]
5. *IEEE Standard 1709-2018*; IEEE Recommended Practice for 1 kV to 35 kV Medium-Voltage DC Power Systems on Ships. IEEE: New York, NY, USA, 2018.
6. Yao, J.; Chen, W.; Xue, C.; Yuan, Y.; Wang, T. An ISOP Hybrid DC Transformer Combining Multiple SRCs and DAB Converters to Interconnect MVDC and LVDC Distribution Networks. *IEEE Trans. Power Electron.* **2020**, *35*, 11442–11452. [CrossRef]
7. Reddy, P.L.S.K.; Obulesu, Y.P. Design and Development of a New Transformerless Multi-port DC–DC Boost Converter. *J. Electr. Eng. Technol.* **2023**, *18*, 1013–1028. [CrossRef]
8. Zhao, B.; Song, Q.; Li, J.; Sun, Q.; Liu, W. Full-Process Operation, Control, and Experiments of Modular High-Frequency-Link DC Transformer Based on Dual Active Bridge for Flexible MVDC Distribution: A Practical Tutorial. *IEEE Trans. Power Electron.* **2017**, *32*, 6751–6766. [CrossRef]
9. Sheng, J.; Chen, C.; Lu, R.; Li, C.; Xiang, X.; Li, W.; He, X. Control Optimization of Modular Multilevel Resonant DC Converters for Wide-Input-Range MVdc to LVdc Applications. *IEEE Trans. Power Electron.* **2022**, *37*, 5284–5298. [CrossRef]
10. Ferreira, J.A. The multilevel modular DC converter. *IEEE Trans. Power Electron.* **2013**, *28*, 4460–4465. [CrossRef]
11. Jovcic, D. Bidirectional, high-power DC transformer. *IEEE Trans. Power Deliv.* **2009**, *24*, 2276–2283. [CrossRef]
12. Li, W.; He, X. Review of Nonisolated High-Step-Up DC/DC Converters in Photovoltaic Grid-Connected Applications. *IEEE Trans. Ind. Electron.* **2011**, *58*, 1239–1250. [CrossRef]
13. Stieneker, M.; De Doncker, R.W. Medium-voltage DC distribution grids in urban areas. In Proceedings of the 2016 IEEE 7th International Symposium on Power Electronics for Distributed Generation Systems (PEDG), Vancouver, BC, Canada, 27–30 June 2016; IEEE: Vancouver, BC, Canada, 2016; pp. 1–7. [CrossRef]
14. Luth, T.; Merlin, M.M.C.; Green, T.C.; Hassan, F.; Barker, C.D. High-Frequency Operation of a DC/AC/DC System for HVDC Applications. *IEEE Trans. Power Electron.* **2014**, *29*, 4107–4115. [CrossRef]
15. Wang, X.; Peng, Y.; Chai, J.; Xia, Y.; Wei, W.; Yu, M. An Ideal DC Transformer for Active DC Distribution Networks Based on Constant-Transformation-Ratio DABC. *IEEE Trans. Power Electron.* **2020**, *35*, 2170–2183. [CrossRef]
16. Zhao, B.; Song, Q.; Liu, W.; Sun, Y. Overview of Dual-Active-Bridge Isolated Bidirectional DC–DC Converter for High-Frequency-Link Power-Conversion System. *IEEE Trans. Power Electron.* **2014**, *29*, 4091–4106. [CrossRef]
17. Alhurayyis, I.; Elkhateb, A.; Morrow, J. Isolated and Nonisolated DC-to-DC Converters for Medium-Voltage DC Networks: A Review. *IEEE J. Emerg. Sel. Top. Power Electron.* **2021**, *9*, 7486–7500. [CrossRef]
18. Xiang, X.; Gu, Y.; Qiao, Y.; Zhang, X.; Li, W.; He, X.; Green, T.C. Resonant Modular Multilevel DC–DC Converters for Both High and Low Step-Ratio Connections in MVDC Distribution Systems. *IEEE Trans. Power Electron.* **2021**, *36*, 7625–7640. [CrossRef]
19. Zhao, B.; Li, X.; Wei, Y.; An, F.; Sun, J.; Liu, G.; Zhao, Y. Modular Hybrid-Full-Bridge DC Transformer with Full-Process Matching Switching Strategy for MVdc Power Distribution Application. *IEEE Trans. Ind. Electron.* **2020**, *67*, 3317–3328. [CrossRef]
20. Du, S.; Wu, B.; Tian, K.; Xu, D.; Zargari, N.R. A Novel Medium-Voltage Modular Multilevel DC–DC Converter. *IEEE Trans. Ind. Electron.* **2016**, *63*, 7939–7949. [CrossRef]
21. Gray, P.A.; Lehn, P.W.; Yakop, N. A Modular Multilevel DC–DC Converter with Flying Capacitor Converter Like Properties. *IEEE Trans. Ind. Electron.* **2022**, *69*, 6774–6783. [CrossRef]
22. Xing, D.; Hu, B.; Li, X.; Cheng, Q.; Wang, J.; Atcitty, S. Comparison of Modular Multilevel Converter Based High Voltage-Step-Down Ratio DC/DC Converters for Energy Storage System Applications. *IEEE J. Emerg. Sel. Top. Power Electron.* **2023**. [CrossRef]
23. Falin, J.; Aguilar, A. Maximize power density with three-level buck-switching charges. *Analog. Des. J. Q* **2021**, 1–8.
24. Meynard, T.A.; Foch, H. Multi-level conversion: High voltage choppers and voltage-source inverters. In Proceedings of the PESC '92 Record, 23rd Annual IEEE Power Electronics Specialists Conference, Toledo, Spain, 29 June–31 July 1992; 1992; Volume 1, pp. 397–403. [CrossRef]
25. Stupar, A.; McRae, T.; Vukadinović, N.; Prodić, A.; Taylor, J.A. Multi-Objective Optimization of Multi-Level DC–DC Converters Using Geometric Programming. *IEEE Trans. Power Electron.* **2019**, *34*, 11912–11939. [CrossRef]
26. Ye, Z.; Lei, Y.; Liao, Z.; Pilawa-Podgurski, R.C.N. Investigation of Capacitor Voltage Balancing in Practical Implementations of Flying Capacitor Multilevel Converters. *IEEE Trans. Power Electron.* **2022**, *37*, 2921–2935. [CrossRef]
27. Villar, G.; Alarcon, E. Monolithic Integration of a 3-Level DCM-Operated Low-Floating-Capacitor Buck Converter for DC-DC Step-Down Conversion in Standard CMOS. In Proceedings of the 2008 IEEE Power Electronics Specialists Conference, Rhodes, Greece, 15–19 June 2008. [CrossRef]

28. Denniston, N.; Massoud, A.M.; Ahmed, S.; Enjeti, P.N. Multiple-Module High-Gain High-Voltage DC–DC Transformers for Offshore Wind Energy Systems. *IEEE Trans. Ind. Electron.* **2011**, *58*, 1877–1886. [CrossRef]
29. Athab, H.; Yazdani, A.; Wu, B. A transformerless DC-DC converter with large voltage ratio for MV DC grids. *IEEE Trans. Power Deliv.* **2014**, *29*, 1877–1885. [CrossRef]
30. Abbasi, M.; Emamalipour, R.; Cheema, M.A.M.; Lam, J. A Constant-Frequency High-Voltage Gain Resonant Converter Module with Semiactive Phase-Shifted Voltage Multiplier for MVdc Distribution. *IEEE J. Emerg. Sel. Top. Power Electron.* **2022**, *10*, 3603–3616. [CrossRef]
31. Zheng, L.; Kandula, R.P.; Divan, D. Current-Source Solid-State DC Transformer Integrating LVDC Microgrid, Energy Storage, and Renewable Energy into MVDC Grid. *IEEE Trans. Power Electron.* **2022**, *37*, 1044–1058. [CrossRef]
32. Li, L.; Jiang, Z.; Jiang, Y. A SEPIC Flyback DC-DC Converter with GaN Switching Device. *J. Electr. Eng. Technol.* **2023**, *18*, 2759–2769. [CrossRef]